NLTT 5306: the shortest period detached white dwarf+brown dwarf binary

P. R. Steele,[1]⋆ R. P. Saglia,[1] M. R. Burleigh,[2] T. R. Marsh,[3] B. T. Gänsicke,[3] K. Lawrie,[2] M. Cappetta,[1] J. Girven[3] and R. Napiwotzki[4]

[1]*Max-Planck-Institut für extraterrestrische Physik, Giessenbachstrasse, D-85748 Garching, Germany*
[2]*Department of Physics and Astronomy, University of Leicester, University Road, Leicester LE1 7RH, UK*
[3]*Department of Physics, University of Warwick, Coventry CV4 7AL, UK*
[4]*Centre for Astrophysics Research, University of Hertfordshire, College Lane, Hatfield AL10 9AB, UK*

ABSTRACT

We have spectroscopically confirmed a brown dwarf mass companion to the hydrogen atmosphere white dwarf NLTT 5306. The white dwarf's atmospheric parameters were measured using the Sloan Digital Sky Survey and X-shooter spectroscopy as $T_{\rm eff} = 7756 \pm 35$ K and $\log(g) = 7.68 \pm 0.08$, giving a mass for the primary of $M_{\rm WD} = 0.44 \pm 0.04\,{\rm M}_\odot$ at a distance of 71 ± 4 pc with a cooling age of 710 ± 50 Myr. The existence of the brown dwarf secondary was confirmed through the near-infrared arm of the X-shooter data and a spectral type of dL4–dL7 was estimated using standard spectral indices. Combined radial velocity measurements from the Sloan Digital Sky Survey, X-shooter and the Hobby–Eberly Telescope's High Resolution Spectrograph of the white dwarf give a minimum mass of $56 \pm 3\,M_{\rm Jup}$ for the secondary, confirming the substellar nature. The period of the binary was measured as 101.88 ± 0.02 min using both the radial velocity data and i'-band variability detected with the Isaac Newton Telescope. This variability indicates 'day' side heating of the brown dwarf companion. We also observe Hα emission in our higher resolution data in phase with the white dwarf radial velocity, indicating that this system is in a low level of accretion, most likely via a stellar wind. This system represents the shortest period white dwarf+brown dwarf binary and the secondary has survived a stage of common envelope evolution, much like its longer period counterpart, WD 0137−349. Both systems likely represent bona fide progenitors of cataclysmic variables with a low-mass white dwarf and a brown dwarf donor.

Key words: brown dwarfs – stars: low-mass – white dwarfs – infrared: stars.

1 INTRODUCTION

As the descendants of high-mass-ratio binaries, brown dwarf (BD) companions to white dwarfs (WDs) enable investigation of one extreme of binary formation and evolution, including the known deficit of BD companions to main-sequence stars (McCarthy & Zuckerman 2004; Grether & Lineweaver 2006). The BDs can be directly detected relatively easily at all separations, since they dominate the spectral energy distribution (SED) at near- to mid-infrared wavelengths, in stark contrast to main-sequence+substellar pairs.

As detached companions to WDs, BDs are rare (∼0.5 per cent; Girven et al. 2011; Steele et al. 2011). Only a handful of such systems have thus far been spectroscopically confirmed, e.g. GD165 (DA+dL4; Becklin & Zuckerman 1988), GD 1400 (DA+dL6–dL7;

Farihi & Christopher 2004; Dobbie et al. 2005), WD 0137−349 (DA+dL8; Burleigh et al. 2006; Maxted et al. 2006), PHL 5038 (DA+dL8; Steele et al. 2009) and LSPM 1459+0857 (DA+T4.5; Day-Jones et al. 2011). GD 165, PHL 5038 and LSPM 1459+0857 can be classed as widely orbiting with projected separations of 120, 55 and 16500–26500 au, respectively. WD 0137−349 and GD 1400 have much shorter orbital periods of 116 min and ∼10 h (Burleigh et al. 2011), respectively, and have both undergone a common envelope evolution.

These two distinct populations are thought to be the outcome of stellar evolution: the wide pairs where the secondary has migrated outwards due to the mass-loss of the WD's progenitor (Farihi, Hoard & Wachter 2006; Nordhaus et al. 2010), and the close systems in which the secondary has survived a stage of common envelope evolution and may eventually lead to the formation of a cataclysmic variable (CV; Politano 2004a). In these close binaries, the BD is expected to be irradiated by the WD's high UV flux, leading to

⋆ E-mail: psteele@mpe.mpg.de

Table 1. SDSS and UKIDSS magnitudes of NLTT 5306.

Band	Magnitude
u'	17.51 ± 0.01
g'	17.03 ± 0.00
r'	16.95 ± 0.00
i'	16.96 ± 0.01
z'	17.00 ± 0.01
Y	16.49 ± 0.01
J	16.24 ± 0.01
H	15.86 ± 0.01
K	15.56 ± 0.02

substantial differences in the 'day' and 'night' side hemispheres. These systems can additionally be used for testing models of irradiated 'hot Jupiter' atmospheres (e.g. HD 189733b; Knutson et al. 2007).

NLTT 5306 (SDSS J 013532.98+144555.8) was first identified as a candidate WD+BD binary in Steele et al. (2011) and Girven et al. (2011). The former used an estimate of the WD's atmospheric parameters ($T_{eff} = 8083 \pm 22$ and $\log g = 8.08 \pm 0.04$; Eisenstein et al. 2006) in combination with cooling models for hydrogen atmosphere (DA) WDs (Holberg & Bergeron 2006; Kowalski & Saumon 2006; Bergeron et al. 2011; Tremblay, Bergeron & Gianninas 2011) to predict the star's near-infrared (NIR) photometry. A comparison was then made with the UKIRT Infrared Deep Sky Survey, Lawrence et al. 2007 (UKIDSS) observations identifying NLTT 5306 as having an NIR excess consistent with a red companion. The Sloan Digital Sky Survey (SDSS) and UKIDSS magnitudes are given in Table 1. Further fitting of the photometry yielded an estimated spectral type of dL5 for the secondary, with a mass of $58 \pm 2 M_{Jup}$ at a distance of 60 ± 10 pc. It should be noted that this spectroscopic mass estimate is model dependent, calculated by interpolating the Lyon group atmospheric models (Chabrier et al. 2000; Baraffe et al. 2002) given an estimated age for the WD and temperature for the BD. The system was unresolved with an upper limit on the projected separation of <57 au between components.

The structure of this paper is as follows. In Section 2, we describe the observations and their reduction. In Section 3, we describe the analysis of the data, starting with the optical light curve, followed by the optical and NIR spectroscopy of the WD and BD, and finally the radial velocity. In Section 4, we discuss the implications of the results and state our conclusions.

2 OBSERVATIONS AND DATA REDUCTION

2.1 INT optical photometry

NLTT 5306 was observed photometrically for 2 h (80 × 90 s exposures) in the Sloan i'-band on the night of 2009 October 23 with the Wide Field Camera on the 2.5 m Isaac Newton Telescope (INT) in La Palma, Spain. The data were reduced using the INT Wide Field Survey pipeline (Irwin & Lewis 2001) developed by the Cambridge Astronomical Survey Unit. For a detailed description of the reduction process, see Irwin et al. (2007). In brief, a standard CCD reduction was performed by correcting for the bias, trimming the frames, correcting non-linearity, flat-fielding and correcting for the gain. The flux was measured in each observation using aperture photometry and the result converted to magnitudes using nightly zero-point estimates based on standard star field observations (Irwin et al. 2007).

2.2 X-shooter spectroscopy

NLTT 5306 was observed using X-shooter (D'Odorico et al. 2006) mounted at the Very Large Telescope Unit Telescope 2 (VLT-UT2) telescope on the night of 2010 September 5. X-shooter is a medium-resolution spectrograph capable of observing using three independent arms simultaneously: the ultraviolet (UVB), optical (VIS) and the NIR arms covering a wavelength range of 0.3–2.5 μm. For our observations we used slit widths of 0.8, 0.9 and 0.9 arcsec in the UVB, VIS and NIR arms, respectively. Exposure times for each arm were 1200 s in the UVB, 1200 s in the VIS and 12 × 150 s in the NIR. We nodded between each exposure along the NIR slit to improve sky subtraction. This gave us a total of four exposures in each arm.

Reduction of the raw frames was carried out using the standard pipeline release of the European Southern Observatory X-shooter Common Pipeline Library recipes (version 1.3.7) within GASGANO,[1] version 2.4.0. The standard recipes were used with the default settings to reduce and wavelength calibrate the two-dimensional spectrum for each arm. The extraction of the science and spectrophotometric standard and telluric spectra were carried out using APALL within IRAF. The instrumental response was determined by dividing the associated standard star by its corresponding flux table. We also used this method to apply the telluric correction.

Finally, the spectra were flux calibrated using the SDSS and UKIDSS magnitudes (Table 1).

2.3 SDSS spectroscopy

NLTT 5306 was observed on multiple occasions by the SDSS (SDSS J013532.97+144555.9). From the SDSS archive we extracted a total of 17 spectra taken over the period from 2000 December 1 to 20. All but three of these spectra had exposure times of 15 min; the three spectra acquired on December 4 were exposed for 20 min.

2.4 High-resolution spectroscopy with the Hobby–Eberly Telescope

NLTT 5306 was observed using the High Resolution Spectrograph (HRS; Tull 1998) on the Hobby–Eberly Telescope (HET; Ramsey 1998) on the nights of 2010 December 6 and 10, 2011 January 16 and 23, and 2011 February 8. The ephemeris of the system was unknown at the time and so six random observations were taken in order to establish if the primary has a measurable radial velocity variation, and to then estimate an orbital period. Each observation was split into two separate exposures of 1320 s. A ThAr lamp exposure was taken both before and after the science observations in order to aid wavelength calibration.

The cross-disperser setting was '316g5936' corresponding to a wavelength range of 4076–7838 Å, in order to cover the Hα, Hβ and Hγ Balmer lines. This gave a spectral resolving power of $R = \lambda/\delta\lambda = 15\,000$. Two sky fibres were used to simultaneously record the sky background.

Reduction of the raw frames was carried out using standard routines in IRAF. In brief, a bias and flat frames were combined and used to correct the science frames. The extraction of the science spectra was carried out using APALL within IRAF. The sky spectrum was extracted in the same way as the science, simply by shifting all the apertures by a set amount to cover the parallel sky fibre.

[1] http://www.eso.org/sci/software/gasgano

The extracted sky spectrum was then scaled so that the sky lines matched the strength of the corresponding lines in the science spectra. Particular attention was paid to the order containing the Hα absorption. This was then subtracted from the science spectra. Finally, the sky-subtracted science spectra were normalized using the CONTINUUM package within IRAF.

3 ANALYSIS

3.1 Optical light curve

The INT i'-band light curve of NLTT 5306 (Fig. 2) shows low-level photometric variability with a peak-to-peak amplitude of ≈0.8 per cent. The analysis leading to this result is outlined below.

A 'floating-mean' periodogram was used to search for periodicity in the target (Cumming, Marcy & Butler 1999). This method involves fitting the time series data with a sinusoid plus a constant A in the form of

$$A + B \sin[2\pi f(t - t_0)], \tag{1}$$

where f is the frequency and t is the time of observation. The resulting periodogram is a χ^2 plot of the fit with frequency (Fig. 1). The errors associated with the best-fitting frequency were estimated as the 2σ frequency range from the global minimum (corresponding to a change in χ^2 of 4, assuming only one useful fitted parameter).

To evaluate the significance of the best-fitting period, a false alarm probability (FAP) was estimated using 100 000 Monte Carlo trials and an analytical approach for comparison. Fake light-curve data sets were generated for the Monte Carlo tests at the same timings as the observations with the mean magnitude as the observed data. Random Gaussian noise was then added to the flux distributed with the same variance as the observed magnitudes. The FAP was determined from the number of trials where the maximum power in the periodogram (from the fake data set) exceeded the maximum power from the observed data set. A significant detection threshold was set at 1 per cent (FAP $\leq$ 0.01). The analytical probability was determined using the equation given in table 1 in Zechmeister & Kürster (2009) for the residual variance normalization (also see appendix B in Cumming et al. 1999). Further details on the significance tests can be found in Cumming et al. (1999) and Lawrie et al. (in preparation).

A global minimum in the periodogram is found at a frequency of $14.1^{+0.9}_{-1.4}$ cycles d^{-1} and a period of $102.2^{+11.3}_{-6.4}$ min. A fitted sine
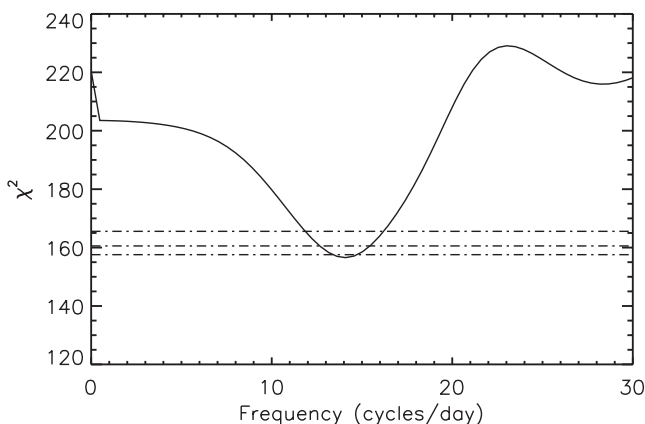
Figure 2. Phase-folded INT i'-band light curve of NLTT 5306 showing a peak-to-peak variability of ∼1 per cent with a period of $102.2^{+11.3}_{-6.4}$ min.

wave to the data gives a reduced χ^2 of 2.07 [χ^2 of 157 over 76 degrees of freedom (d.o.f.)], while a constant fit to the data gives a reduced χ^2 of 2.92 (χ^2 of 231 over 79 d.o.f.). The FAP statistics are well within the limit for a significant detection, with an FAP of <0.001 from the Monte Carlo tests and an FAP of 5×10^{-5} from the analytical estimation. This suggests that it is significantly unlikely that the variability seen in the light curve is due to noise fluctuations alone.

The probability that this system has an alignment that would result in an eclipse as viewable from Earth is ∼20 per cent, with an eclipse duration of ∼7 min (Faedi et al. 2011). No eclipse or grazing transit is immediately obvious in the phase-folded light curve of NLTT 5306 (Fig. 2). Given the total time between exposures of 90 s and the coverage of ∼1.5 orbital periods, it seems unlikely that we would have missed an eclipse.

3.2 WD spectroscopy

Figs 3 and 4 show the extracted X-shooter spectrum for NLTT 5306 separated into the UVB/VIS and NIR arms. This clearly shows the WD primary dominating the optical wavelengths and the BD companion dominating the NIR wavelengths. A closer inspection of

Figure 1. Floating-mean periodogram for the INT i'-band photometry of NLTT 5306. The global minimum is located at a frequency of $14.1^{+0.9}_{-1.4}$ cycles d^{-1}.
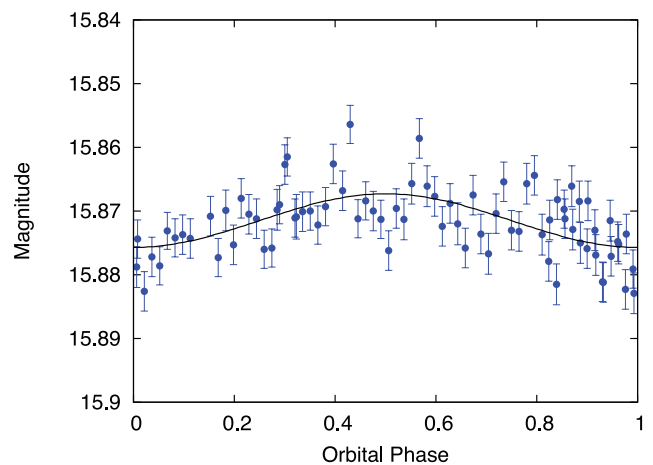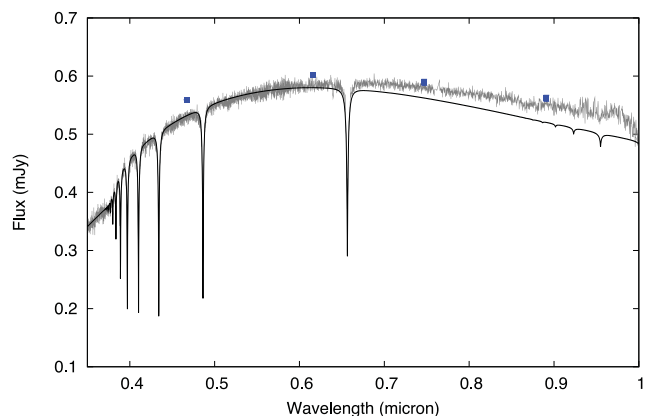
Figure 3. X-shooter spectrum (grey) of WD 0132+142 covering the UVB and VIS arms where the WD primary dominates. SDSS *ugriz* photometry is overplotted (squares). The WD model SED (black) begins to diverge from the observed spectrum at longer wavelengths due to the added flux from the secondary.
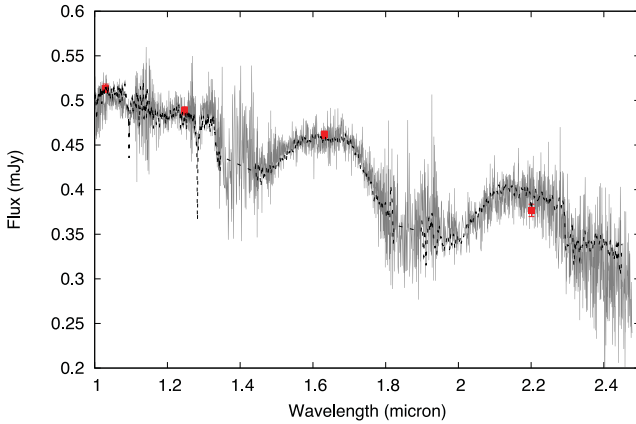
Figure 4. X-shooter spectrum (grey) of WD 0132+142 covering the NIR arm where the BD secondary dominates. UKIDSS *YJHK* photometry is overplotted (squares) as well as a composite WD+dL5 model (black dashed) for visual comparison.
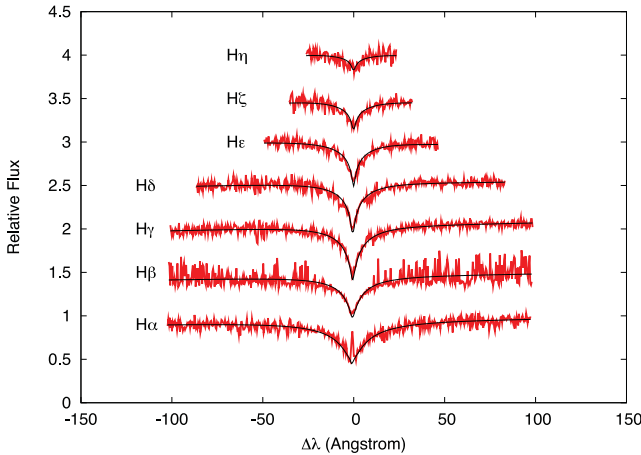

Figure 5. Balmer line fit (black) of NLTT 5306 A using the X-shooter spectrum (grey). The emission line seen at the core of Hα is likely due to accretion via a stellar wind. The region of the emission line was excluded from the fit.

Table 2. Measured atmospheric parameters for NLTT 5306 A from various spectroscopic observations.

Telescope/instrument	T_{eff} (K)	$\log g$	M_{WD} (M$_\odot$)	d (pc)
SDSS 1	7641 ± 48	7.61 ± 0.10	0.39 ± 0.05	72 ± 4
SDSS 2	7729 ± 7	7.67 ± 0.05	0.42 ± 0.02	68 ± 2
SDSS 3	7729 ± 49	7.71 ± 0.10	0.44 ± 0.05	68 ± 4
VLT+X-shooter	7925 ± 15	7.74 ± 0.02	0.47 ± 0.01	70 ± 1

the Hα absorption line in individual exposures revealed the presence of line emission close to the line centre (Fig. 5).

Fig. 5 and Table 2 show the results of fitting the Balmer series with atmospheric models of hydrogen atmosphere DA WDs (Koester 2008), for both the SDSS and X-shooter spectra. The average of these values yields an effective temperature and a surface gravity of $T_{\mathrm{eff}} = 7756 \pm 35$ K and $\log g = 7.68 \pm 0.08$, respectively. We interpolated these values over a grid of synthetic colours and evolutionary sequences of DA WDs[2] to calculate a mass of $M_{\mathrm{WD}} =$

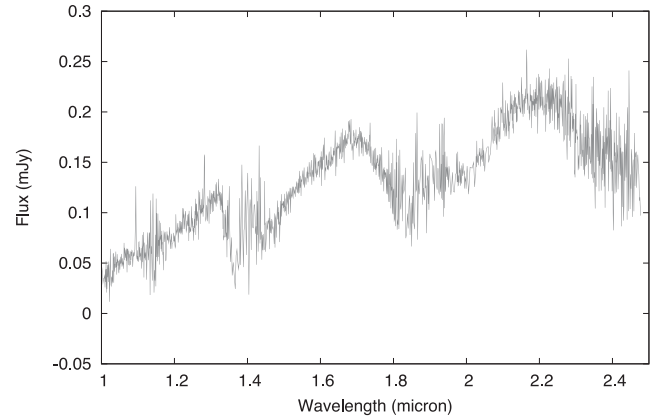[2] http://www.astro.umontreal.ca/~bergeron/CoolingModels/

Figure 6. X-shooter spectrum of NLTT 5306 B (grey) created by subtracting the WD model spectrum calculated using the measured atmospheric parameters of the primary.

0.44 ± 0.04 M$_\odot$ and a distance of 71 ± 4 pc. The results are summarized in Table 4. The region within Hα containing the core emission was excluded from this fit. A model spectrum calculated using these values is overplotted in Fig. 3.

It should be noted that the spectroscopic fit may have led to an overestimate of the WD's mass, due to the difficulty in modelling the hydrogen line profiles below $T_{\mathrm{eff}} \approx 12\,000$–$13\,000$ K. The Tremblay et al. (2011) analysis of SDSS WDs suggests an overestimate at the level of 10 per cent, although this is largely based on WDs with a mass of around 0.6 M$_\odot$. A lower WD mass would decrease the minimum value for the mass of the secondary, relaxing the need for the system to have a high inclination for the mass to be consistent with the spectral type of dL4–dL7 and given the non-detection of an eclipse or grazing transit (Section 3.1).

3.3 BD spectroscopy

The model WD spectrum for NLTT 5306 A was subtracted from the observed X-shooter spectrum in order to estimate the SED of solely the secondary, NLTT 5306 B (Fig. 6).

In order to estimate a spectral type for the secondary, we have calculated the H$_2$O$^{\mathrm{b}}$ and H$_2$O$^{\mathrm{c}}$ indices, defined by

$$H_2O^b = F(1.48)/F(1.60) \qquad (2)$$

$$H_2O^c = F(1.80)/F(1.70). \qquad (3)$$

Here F is the average flux in a band, with ± 0.01 μm, centred on the specified wavelength. Burgasser et al. (2002) state that the H$_2$O$^{\mathrm{b}}$ index in particular shows a linear relation with spectral type given by

$$\mathrm{SpT} = (12.6 \pm 0.9) - (26.7 \pm 0.6)\ H_2O^b, \qquad (4)$$

where SpT $= 0$ at dT0 and SpT $= -4$ at dL5. This relation holds for spectral types between dM5 (-14) and dT8 (8).

Fig. 7 shows these indices as measured for L-dwarfs from the NIRSPEC infrared archive,[3] as well as the H$_2$O$^{\mathrm{b}} = 0.637$ and H$_2$O$^{\mathrm{c}} = 0.627$ as measured for NLTT 5306 B. Substituting the former value into equation (4) gives SpT $= -4.4 \pm 1.3$, corresponding to a spectral type between dL4 and dL7. This is consistent with the original photometry-based spectral type estimate of dL5 in Steele et al. (2011).
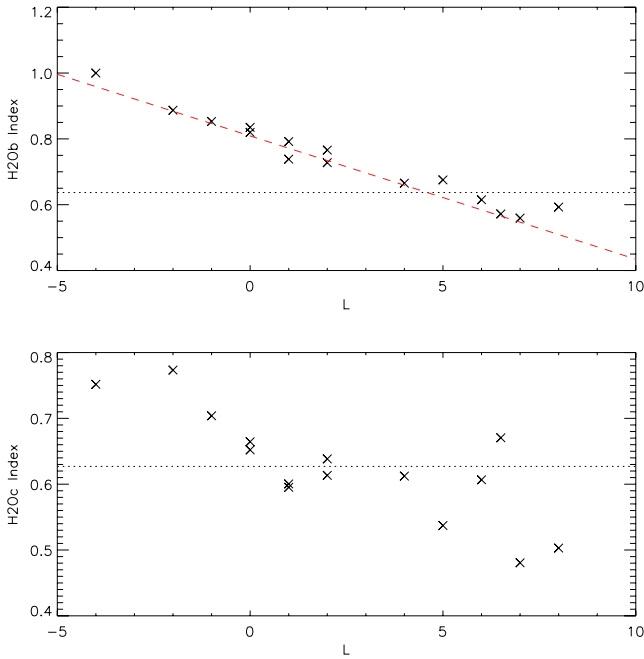
[3] http://www.astro.ucla.edu/mclean/BDSSarchive/

Figure 7. H_2O^b and H_2O^c indices as measured for L-dwarfs from the NIRSPEC infrared archive (crosses). The short-dashed lines show the same indices measured for NLTT 5306 B. These suggest the spectral type in the approximate range dL4–dL7. The H_2O^b index (upper panel) is the better indicator of the spectral type. Equation (4) is overplotted in the upper panel (long-dashed) to show the linear relationship between spectral type and the H_2O^b index.

3.4 Radial velocity

Each SDSS spectrum is a combination of separate red and blue components. We split these into two data sets, the first covering $H\alpha$ and the second covering the higher Balmer series. We fitted multiple Gaussian components to these lines, using two Gaussians per line (see Marsh, Dhillon & Duck 1995 for details of this process). Once profiles to the mean spectra had been fitted, then for the final fit we kept all shape parameters fixed and simply allowed the radial velocity to be fitted, giving us our final radial velocities.

The HET spectra also consist of separate blue and red components, the blue end covering $H\beta$ and $H\gamma$, and the red covering $H\alpha$. Four of the five observations consisted of two separate exposures of 1320 s each, with the final observation only producing one such exposure. As these exposures sampled a significant fraction of the orbital period of NLTT 5306 B, each observation was fitted separately, giving a total of nine data points. Four more radial velocities were measured by extracting individually the spectra which were combined to make the final X-shooter spectrum.

The absorption lines in the HET and X-shooter data were fitted using a combination of two Gaussians using the program FITSB2 written by Ralf Napiwotzki. The best-fitting shape parameters were fixed and then fitted for velocity shifts.

The final measured radial velocities for all three data sets are given in Table 3. The SDSS data were shifted so that the mean velocity matched that of the higher resolution and therefore superior HET and X-shooter data. The low resolution of the SDSS data made measurement of the systemic velocity with just the SDSS data unreliable, with a significant difference measured in the mean velocities ($\sim 20\,\mathrm{km\,s^{-1}}$) even between the blue and red arms. The mean velocity measured from HET and X-shooter is consistent with

Table 3. Observation times and measured radial velocities from the Balmer absorption lines of NLTT 5306. The SDSS data have been shifted to the mean systemic velocity of the X-shooter and HET observations.

Telescope/instrument	HJD	RV (km s^{-1})
SDSS	245 1879.737 22	-39.06 ± 14.4
	245 1879.749 35	-57.86 ± 14.6
	245 1879.785 91	58.64 ± 17.7
	245 1882.754 29	51.24 ± 9.8
	245 1882.770 06	29.84 ± 9.9
	245 1882.786 09	-46.46 ± 11.5
	245 1884.671 57	48.14 ± 11.0
	245 1884.683 78	-3.96 ± 11.7
	245 1884.695 93	-52.26 ± 10.9
	245 1884.708 08	-17.46 ± 12.2
	245 1884.720 14	10.94 ± 12.2
	245 1884.732 26	44.64 ± 13.8
	245 1884.744 98	37.34 ± 11.9
	245 1884.757 13	-12.76 ± 11.9
	245 1898.680 69	28.84 ± 8.6
	245 1898.692 85	-11.86 ± 9.1
	245 1898.705 04	-46.76 ± 9.0
VLT+X-shooter	245 5444.860 40	-43.01 ± 4.50
	245 5444.869 33	-12.61 ± 4.94
	245 5444.878 19	16.90 ± 4.72
	245 5444.887 11	43.71 ± 4.65
HET+HRS	245 5536.741 82	-26.24 ± 4.13
	245 5536.757 32	-59.02 ± 6.34
	245 5540.727 58	-29.01 ± 4.09
	245 5540.743 09	19.97 ± 6.01
	245 5577.621 59	27.81 ± 4.50
	245 5577.637 07	-9.44 ± 4.58
	245 5584.613 00	59.44 ± 5.11
	245 5584.628 52	51.29 ± 8.52
	245 5600.575 43	-23.57 ± 5.74

the systemic velocity of $-15 \pm 36\,\mathrm{km\,s^{-1}}$ previously measured in Adelman-McCarthy (2008).

The high resolution of HET HRS and X-shooter spectra allowed for the detection of the line emission in the core of $H\alpha$. The fit to the WD's $H\alpha$ absorption line was used to subtract the contribution of the WD. The emission line was then fitted with a single Gaussian to measure the radial velocity. This was possible in all four X-shooter exposures and eight of the nine HET exposures, with the eighth exposure being too noisy to accurately identify the emission.

Periodicity was searched for in the combined radial velocity data (Table 3) of the WDs' absorption lines (SDSS, HET and X-shooter) and for the line emission (HET and X-shooter) using the method discussed in Section 3.1. For the WD, 30 unique data points were used as measured from the Balmer series absorption lines, and 12 as measured from the line emission in the core of $H\alpha$.

Fig. 8 shows the periodogram for the fit of the WD radial velocity measurements. The analysis of this data resulted in two favoured aliases with periods of 109.96 ± 0.02 min ($\chi^2 = 72.6$) and 101.88 ± 0.02 min ($\chi^2 = 66.5$). The χ^2 value slightly favours the shorter period alias which would be consistent with the period measured from the INT light curve. However, the longer period alias produces a period which is also within errors of this value. Therefore, it was not possible to determine the period accurately just utilizing the available WD data.

Fig. 9 shows the periodogram for the fit of the $H\alpha$ core emission radial velocity measurements. The two most favoured periods of
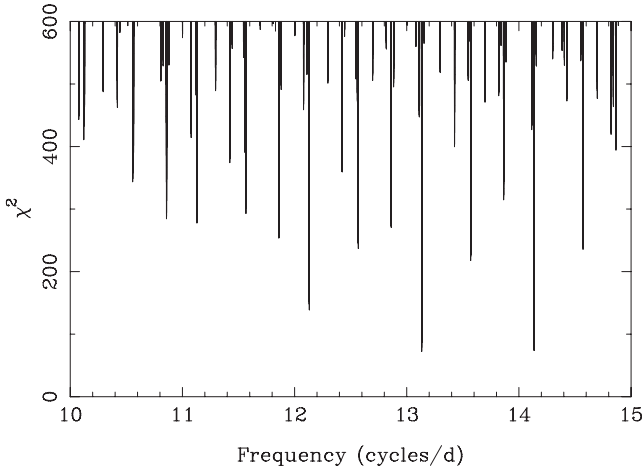
Figure 8. Periodogram covering the region of interest for the WD's radial velocities as measured using the Balmer series absorption lines in the SDSS, HET and X-shooter data. Two aliases are favoured at periods of 101.88 ± 0.02 and 109.96 ± 0.02 min with a minimal difference in χ^2.

101.87 ± 0.04 min ($\chi^2 = 78.5$) and 109.64 ± 0.04 min ($\chi^2 = 93.0$) are indeed consistent with those obtained for both the light curve and the radial velocity fit of the WD. However, the χ^2 value is much more in favour of the shorter period alias in this case. Therefore, we take the value of $P = 101.88 ± 0.02$ min from the larger (and therefore more accurate) absorption line data set for the period of the system.

An attempt was made to measure the radial velocity of the BD component using the four individual X-shooter observations in the NIR arm. Each spectrum was extracted and flux calibrated, and the telluric correction applied. The model WD spectrum (Fig. 3) was then subtracted from each spectrum as in Section 3.3. We then cross-correlated each spectrum with a dL5 template using the IRAF package FXCOR. This was attempted using various wavelength ranges in order to negate the water vapour bands. However, the S/N in the individual exposures was such that the cross-correlations with the template did not produce any sensible results. We also suspect that we were not entirely able to remove the WD contribution satisfactorily, and it is also possible that the BD spectrum undergoes
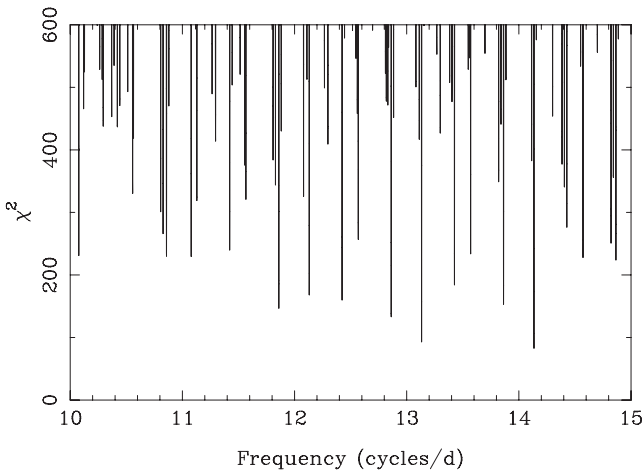

Figure 9. Periodogram covering the region of interest for the BD's radial velocities as measured using the Hα core emission in the HET and X-shooter data. In this case, the periodogram favours the higher frequency alias giving a period of 101.87 ± 0.04 min.

short-term changes in overall shape due to the irradiation from the primary.

4 DISCUSSION

The stellar/substellar nature of an object is dependent on its mass (Kumar 1963). The commonly used limit to distinguish between low-mass main-sequence stars and BDs is $0.075\,M_\odot(75\,M_{Jup};$ Burrows et al. 1997; Chabrier & Baraffe 2000), below which hydrogen fusion does not occur.

Figs 10 and 11 show the phase-folded radial velocity measurements for NLTT 5306. The parameters of the spectroscopic orbit are summarized in Table 5. The period measured using the radial velocity data is consistent with the period measured using the variability of the INT i'-band light curve. Using the calculated value for the mass of the primary, $M_{WD} =0.44 ± 0.04\,M_\odot$ (Table 4), the minimum mass of the secondary is $56 ± 3\,M_{Jup}$, consistent with the measured spectral type of dL4–dL7 and confirming that NLTT 5306 B is a
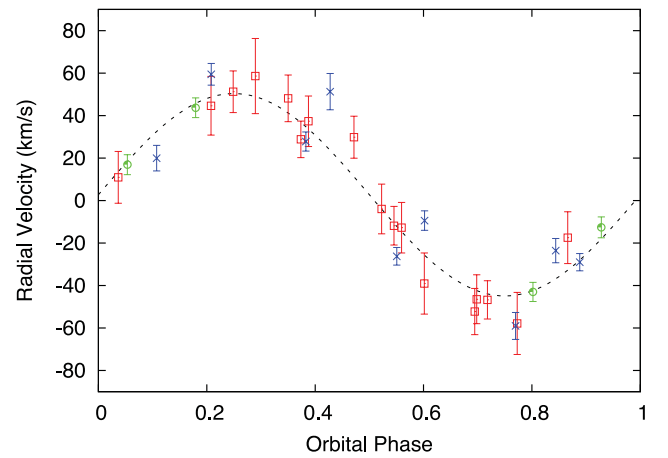

Figure 10. Phase-folded radial velocity curve for the favoured period of 101.87 ± 0.04 min of the hydrogen absorption lines of NLTT 5306 A showing the SDSS (squares), HET (crosses) and X-shooter (circles) data. The curve representing the best-fitting orbital parameters is overplotted (dashed).
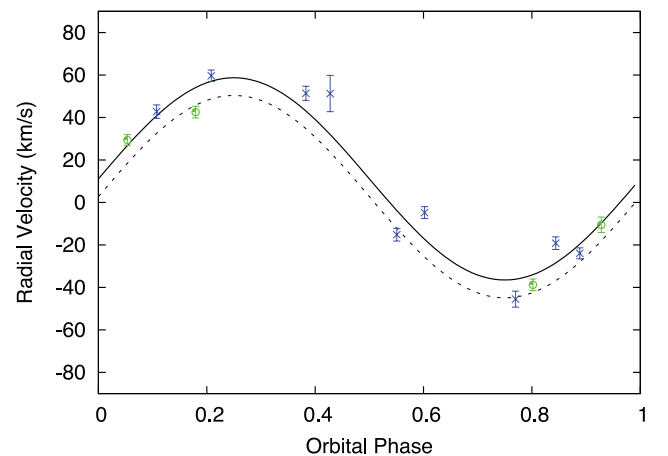

Figure 11. Phase-folded radial velocity curve for the favoured period of 101.87 ± 0.04 min of the Hα emission line showing the HET (crosses) and X-shooter (circles) data. The curve representing the best-fitting orbital parameters is overplotted (solid) as well as the best-fitting model for the absorption lines (dashed).

Table 4. Properties of the white dwarf NLTT 5306 A.

Parameter	Value
T_{eff} (K)	7756 ± 35
$\log g$ (cgs units)	7.68 ± 0.08
Mass ($M_\odot$)	0.44 ± 0.04
Cooling age (Myr)	710 ± 50
Radius ($R_\odot$)	0.0156 ± 0.0016
Distance (pc)	71 ± 4

Table 5. Spectroscopic orbit of NLTT 5306 where the WD radial velocity at a time T is given by $\gamma_1 + K_1 \sin[2\pi f(T - T_0)]$, and the emission line radial velocity by $\gamma_2 + K_2 \sin[2\pi f(T - T_0)]$, where $f = 1/P$ is the frequency.

Parameter	Value
P (min)	101.88 ± 0.02
T_0 (HJD)	$245\ 3740.1408 \pm 0.0005$
K_1 (km s^{-1})	48.1 ± 1.3
K_2 (km s^{-1})	48.9 ± 1.8
γ_1 (km s^{-1})	2.74 ± 1.3
γ_2 (km s^{-1})	11.10 ± 1.0
a ($R_\odot$)	0.566 ± 0.005

bona fide BD. Given this consistency, we suspect that this system has a relatively high inclination, even though no eclipse was detected. It also confirms that NLTT 5306 is the shortest period detached WD+BD binary. Parsons et al. (2012a) detected a detached WD binary system with a period of only 94 min (CSS 03170). However, in this case the secondary has a mass above the hydrogen burning limit and so is classed as a main-sequence star. The most similar known system is WD 0137−349 which has an orbital period of 116 min (Maxted et al. 2006) and a slightly lower mass secondary ($53 \pm 6\ M_{Jup}$; Burleigh et al. 2006a).

One might assume that the Hα emission seen in our spectroscopy is likely to arise from the irradiation of the BD's atmosphere by the WD primary, as is the case for WD 0137−349. If this were true, then the radial velocity measurements would be in antiphase with those measured from the Hα absorption, and the amplitude would allow us to solve for the masses of both binary components. However, Fig. 11 shows that the emission is clearly in phase with the absorption, and with a similar measured amplitude of 48.9 ± 1.8 km s^{-1}, its origin must be associated with the WD. The most likely cause of such emission is accretion, either via Roche lobe overflow or wind from the substellar companion.

Burleigh et al. (2006b) observed a similar situation in the magnetic WD+BD binary SDSS J 121209.31+013627.7 ($P_{orb} \approx$ 90 min). In this case, the system is considered to be in a semidetached state with a magnetic CV (polar) in a low state of accretion from a BD on to a magnetic WD. Although NLTT 5306 shows no evidence of a detectable magnetic field and at $P_{orb} \approx 102$ min is probably not in semidetached contact, it may be accreting from a weak wind from the BD. Therefore, NLTT 5306 is more akin to the wind accreting system LTT 560 (Tappert et al. 2007, 2011b), albeit in this system the secondary is a much earlier spectral type of dM5.

The Hα emission seen in LTT 560 consists of two antiphased components, one originating in the secondary and the other from a chromosphere on the WD as a result of accretion via the companion's stellar wind. NLTT 5306 only shows the emission component associated with the WD, and so we conclude that we may be observing a similar situation where there is only chromospheric emission and no obvious activity from the secondary (which is to be expected given the estimated spectral type). The origin of this emission line component in post-common-envelope binaries (PCEB) is briefly discussed in Tappert et al. (2011a), although given the rarity of systems where the Hα emission line component is located on the WD, it is presently unclear under what conditions chomospheric emission occurs.

If NLTT 5306 is accreting via a stellar wind on to a chromosphere, then this would occur some distance above the WD. The systemic velocity of the observed emission is similar in value to that of the radial velocity measured using the WDs' Balmer absorption lines. Some difference would be expected due to the gravitational redshift of the WD if the emission was chromospheric in origin. Adopting

the measured atmospheric parameters from this work, this amounts to a redshift of $v_{gr} = 17.9 \pm 3.5$ km s^{-1}. Fig. 11 shows that the systemic velocity of the emission feature is $\sim$5–10 km s^{-1} greater than that measured from Balmer absorption. If anything we would expect it to be less (i.e. redshifted compared to the WD) but given the low S/N of the emission detected in the HET data (on which the fit heavily relies), this value should not be trusted. In all likelihood the emission-forming region is somewhere above the WD photosphere. This could be further constrained with more accurate measurements of the radial velocity of the absorption and emission features, and should be considered as a future project for the VLT+X-shooter.

The effective temperature of the BD can be estimated to be $\sim$1700 K from its measured spectral type of dL4–dL7 and comparison with observed L-dwarfs (Vrba et al. 2004). Using this effective temperature and the cooling age of the WD (Table 4) as a minimum value for the age of the system, we have estimated the radius of NLTT 5306 B to be $R_{BD} = 0.95 \pm 0.04\ R_{Jup}$ by interpolating the Lyon group atmospheric models (Chabrier et al. 2000; Baraffe et al. 2002).

The systemic velocity of the WD allows us to discuss the kinematics of the system, in particular the U velocity. This gives a good indication of whether the WD is a thin disc, thick disc or halo object, and thus allows for further constraints on the age of the primary. Using the equations of Johnson & Soderblom (1987) and the values given in Tables 4 and 5, we calculate $U \approx 70$ km s^{-1} for NLTT 5306. This would seem to suggest that the WD is a member of the thick disc population (see fig. 4 of Pauli et al. 2006) and is likely much older than the minimum cooling age suggests (>5 Gyr). At this age the Lyon group models give a mass of closer to 70 M_{Jup} for the companion, still well within the accepted BD range.

The asymmetric heating and rotation of the BD produces a modulation of brightness known as the 'reflection effect' (Wilson 1990). This has been detected at the order of $\sim$1 per cent in the INT i'-band light curve. Since the BD is tidally locked with the WD, this has allowed us to estimate the binary orbital period independently of the radial velocity measurements. A more accurate spectral typing of the companion would require further measurements of this effect at longer wavelengths (i.e. the NIR) where this variation would be more pronounced (Burleigh et al. 2008).

Variability has also been observed in the i' band for WD 0137−349, but of the order of $\sim$2 per cent (Burleigh, private communication). WD 0137−349 A is hotter than NLTT 5306 ($\sim$16 000 K) so there are more UV photons, and more flux overall by approximately an order of magnitude. Therefore, we would not necessarily expect to observe such a strong effect on NLTT 5306 B, which may also depend on local conditions and chemistry in the BD

atmosphere, but a variation of ∼1 per cent seems consistent with the effects of irradiation.

The progenitor system of NLTT 5306 A and NLTT 5306 B consisted of a main-sequence star and a BD with an orbital separation sufficiently small for the progenitor of NLTT 5306 A to fill its Roche lobe as it evolved off the main sequence. As a consequence of the ensuing unstable mass transfer, the BD was engulfed in the envelope of the progenitor of NLTT 5306 A, leading to a rapid reduction in the orbital period and the ejection of the envelope. The low mass of NLTT 5306 A suggests that the core growth was truncated by this common envelope evolution, and that this WD may contain a He core (Webbink 1984; Iben & Tutukov 1986; Rebassa-Mansergas et al. 2011). Therefore, the evolution of NLTT 5306 A likely terminated on the red giant branch rather than the asymptotic giant branch.

Following the emergence from the common envelope, the binary continued to evolve towards shorter periods. Given the low mass of NLTT 5306 B, gravitational wave radiation is likely to be the only relevant agent of orbital angular momentum loss. Adopting the stellar parameters for the WD and the BD determined above, and using the formalism outlined by Schreiber & Gänsicke (2003), we calculate the orbital period at the end of the common envelope to be $P_{CE} \simeq 120$ min. The orbital period of NLTT 5306 will continue to decrease for another ≃900 Myr, until the BD will eventually fill its Roche lobe and initiate stable mass transfer on to the WD. This transformation into a CV will occur at an orbital period of ≃68 min, near the orbital period minimum of CVs (Gänsicke et al. 2008).

The existence of WD 0137−349 B (Burleigh et al. 2006a; Maxted et al. 2006) and NLTT 5306 B demonstrates that BDs can survive common envelope evolution (see also Nordhaus et al. 2010), and their short orbital periods and low WD masses are in line with the statistics of the much larger sample of PCEB containing low-mass M-dwarfs (Zorotovic, Schreiber & Gänsicke 2011a). Binary population models predict both the existence of CVs born at very short periods with BD donors (Politano 2004b) and CVs containing low-mass He-core WDs (e.g. de Kool 1992; Politano 1996). Yet, among the sample of known CVs, there is no compelling evidence for either systems that were born with a BD donor (see the discussion in Littlefair et al. 2007; Uthas et al. 2011; Breedt et al. 2012; Parsons et al. 2012b) or CVs containing low-mass WDs (Savoury et al. 2011; Zorotovic, Schreiber & Gänsicke 2011b). We conclude that WD 0137−349 and NLTT 5306 represent nearby bona fide progenitors of CVs with low-mass WDs and BD donors, and that the lack of such systems among the CV population reflects that the present-day population of pre-CVs is not fully representative of the progenitors of the present-day population of CVs.

5 SUMMARY

We have spectroscopically confirmed the shortest period WD+BD binary known to date. Radial velocity variations and i'-band variability due to 'day' and 'night' side heating of the secondary give us a period of 101.88 ± 0.02 min and a minimum mass for the companion of $56 \pm 3 \, M_{Jup}$. This is consistent with the spectral type estimated from the spectroscopy of dL4–dL7. The results are summarized in Table 5. Emission near the core of Hα indicates accretion either via a stellar wind or via Roche lobe overflow. NLTT 5306 B has survived a stage of common envelope evolution, much like its longer period counterpart WD 0137−349. Both systems are likely to represent bona fide progenitors of CVs with a low-mass WD and a BD donor.

REFERENCES

Adelman-McCarthy J. K. et al., 2008, ApJS, 175, 297
Baraffe I., Chabrier G., Allard F., Hauschildt P. H., 2002, A&A, 382, 563
Becklin E. E., Zuckerman B., 1988, Nat, 336, 656
Bergeron P. et al., 2011, ApJ, 737, 28
Breedt E., Gänsicke B. T., Marsh T. R., Steeghs D., Drake A. J., Copperwheat C. M., 2012, MNRAS, 425, 2548
Burgasser A. J. et al., 2002, ApJ, 564, 421
Burleigh M. R., Hogan E., Dobbie P. D., Napiwotzki R., Maxted P. F. L., 2006a, MNRAS, 373, L55
Burleigh M. R. et al., 2006b, MNRAS, 373, 1416
Burleigh M., Dobbie P., Maxted P., Napiwotzki R., 2008, Anglo-Aust. Obs. Epping Newsl., 114, 17
Burleigh M. R. et al., 2011, in Schuh S., Drechsel H., Heber U., eds, AIP Conf. Ser. Vol. 1331, Brown Dwarf Companions to White Dwarfs. Am. Inst. Phys., New York, p. 262
Burrows A. et al., 1997, ApJ, 491, 856
Chabrier G., Baraffe I., 2000, ARA&A, 38, 337
Chabrier G., Baraffe I., Allard F., Hauschildt P., 2000, ApJ, 542, 464
Cumming A., Marcy G. W., Butler R. P., 1999, ApJ, 526, 890
Day-Jones A. C. et al., 2011, MNRAS, 410, 705
de Kool M., 1992, A&A, 261, 188
Dobbie P. D., Burleigh M. R., Levan A. J., Barstow M. A., Napiwotzki R., Holberg J. B., Hubeny I., Howell S. B., 2005, MNRAS, 357, 1049
D'Odorico S. et al., 2006, Proc. SPIE, 6269
Eisenstein D. J. et al., 2006, ApJS, 167, 40
Faedi F., West R. G., Burleigh M. R., Goad M. R., Hebb L., 2011, MNRAS, 410, 899
Farihi J., Christopher M., 2004, AJ, 128, 1868
Farihi J., Hoard D. W., Wachter S., 2006, ApJ, 646, 480
Gänsicke B. T. et al., 2008, MNRAS, 397, 2170
Girven J., Gänsicke B. T., Steeghs D., Koester D., 2011, MNRAS, 417, 1210
Grether D., Lineweaver C. H., 2006, ApJ, 640, 1051
Holberg J. B., Bergeron P., 2006, AJ, 132, 1221
Iben I., Jr, Tutukov A. V., 1986, ApJ, 311, 742
Irwin M., Lewis J., 2001, New Astron. Rev., 45, 105
Irwin J., Irwin M., Aigrain S., Hodgkin S., Hebb L., Moraux E., 2007, MNRAS, 375, 1449
Johnson D. R. H., Soderblom D. R., 1987, ApJ, 93, 864
Knutson H. A. et al., 2007, Nat, 447, 183
Koester D., 2008, arXiv:0812.0482
Kowalski P. M., Saumon D., 2006, ApJ, 651, L137
Kumar S. S., 1963, ApJ, 137, 1121
Lawrence et al., 2007, MNRAS, 379, 1599
Littlefair S. P., Dhillon V. S., Marsh T. R., Gänsicke B. T., Baraffe I., Watson C. A., 2007, MNRAS, 381, 827
Marsh T. R., Dhillon V. S., Duck S. R., 1995, MNRAS, 275, 828

Maxted P. F. L., Napiwotzki R., Dobbie P. D., Burleigh M. R., 2006, Nat, 442, 543

McCarthy C., Zuckerman B., 2004, AJ, 127, 2871

Nordhaus J., Spiegel D. S., Ibgui L., Goodman J., Burrows A., 2010, MNRAS, 408, 631

Parsons S. G. et al., 2012a, MNRAS, 419, 304

Parsons S. G. et al., 2012b, MNRAS, 419, 304

Pauli E.-M., Napiwotzki R., Heber U., Altmann M., Odenkirchen M., 2006, A&A, 447, 173

Politano M., 1996, ApJ, 465, 338

Politano M., 2004a, ApJ, 604, 817

Politano M., 2004b, ApJ, 604, 817

Ramsey L. W., 1998, BAAS, 30, 185

Rebassa-Mansergas A., Nebot Gómez-Morán A., Schreiber M. R., Girven J., Gänsicke B. T., 2011, MNRAS, 413, 1121

Savoury C. D. J. et al., 2011, MNRAS, 415, 2025

Schreiber M. R., Gänsicke B. T., 2003, A&A, 406, 305

Steele P. R., Burleigh M. R., Farihi J., Gänsicke B. T., Jameson R. F., Dobbie P. D., Barstow M. A., 2009, A&A, 500, 1207

Steele P. R., Burleigh M. R., Dobbie P. D., Jameson R. F., Barstow M. A., Satterthwaite R. P., 2011, MNRAS, 416, 2768

Tappert C., Gänsicke B. T., Schmidtobreick L., Mennickent R. E., Navarrete F. P., 2007, A&A, 475, 575

Tappert C., Gänsicke B. T., Rebassa-Mansergas A., Schmidtobreick L., Schreiber M. R., 2011a, A&A, 531, A113

Tappert C., Gänsicke B. T., Schmidtobreick L., Ribeiro T., 2011b, A&A, 532, A129

Tremblay P.-E., Bergeron P., Gianninas A., 2011, ApJ, 730, 128

Tull R. G., 1998, Proc. SPIE, 3355, 387

Uthas H., Knigge C., Long K. S., Patterson J., Thorstensen J., 2011, MNRAS, 414, L85

Vrba F. J. et al., 2004, AJ, 127, 2948

Webbink R. F., 1984, ApJ, 277, 355

Wilson R. E., 1990, ApJ, 356, 613

Zechmeister M., Kürster M., 2009, A&A, 496, 577

Zorotovic M., Schreiber M. R., Gänsicke B. T., 2011a, A&A, 536, A42

Zorotovic M., Schreiber M. R., Gänsicke B. T., 2011b, A&A, 536, A42

This paper has been typeset from a TeX/LaTeX file prepared by the author.